Brief Communication

Cell Chemical Biology

Metabolic Modifier Screen Reveals Secondary Targets of Protein Kinase Inhibitors within Nucleotide Metabolism

Highlights

- Convergent UMP biosynthetic pathways interchangeably sustain cancer cell proliferation
- Phenotypic screens can identify selective modulators of convergent metabolic networks
- Multiple protein kinase inhibitors possess secondary targets within UMP metabolism

Authors

Evan R. Abt, Ethan W. Rosser, Matthew A. Durst, ..., Timothy R. Donahue, Arnon Lavie, Caius G. Radu

Correspondence

cradu@mednet.ucla.edu

In Brief

Pyrimidine nucleotides are produced interchangeably by convergent metabolic pathways. Abt et al. develop and apply a phenotypic screen that leverages this redundancy to identify selective small-molecule metabolism modifiers. Multiple compounds developed as protein kinase inhibitors were found to possess secondary targets within nucleotide metabolism.

Abt et al., 2020, Cell Chemical Biology *27*, 1–9
January 16, 2020
https://doi.org/10.1016/j.chembiol.2019.10.012

CellPress

Please cite this article in press as: Abt et al., Metabolic Modifier Screen Reveals Secondary Targets of Protein Kinase Inhibitors within Nucleotide Metabolism, Cell Chemical Biology (2019), https://doi.org/10.1016/j.chembiol.2019.10.012

Cell Chemical Biology

Brief Communication

CellPress

Metabolic Modifier Screen Reveals Secondary Targets of Protein Kinase Inhibitors within Nucleotide Metabolism

Evan R. Abt,[1,2,11] Ethan W. Rosser,[2,3,11] Matthew A. Durst,[4,5,11] Vincent Lok,[1,2] Soumya Poddar,[1,2] Thuc M. Le,[1,2] Arthur Cho,[6] Woosuk Kim,[1,2] Liu Wei,[1,2] Janet Song,[1,2] Joseph R. Capri,[1,2] Shili Xu,[2,7] Nanping Wu,[2,7] Roger Slavik,[1,2] Michael E. Jung,[3] Robert Damoiseaux,[1,8] Johannes Czernin,[1,2] Timothy R. Donahue,[1,2,7,9,10] Arnon Lavie,[4,5] and Caius G. Radu[1,2,12,*]

[1]Department of Molecular and Medical Pharmacology, University of California Los Angeles, Los Angeles, CA, USA
[2]Ahmanson Translational Imaging Division, University of California Los Angeles, Los Angeles, CA, USA
[3]Department of Chemistry and Biochemistry, University of California Los Angeles, Los Angeles, CA, USA
[4]Department of Biochemistry and Molecular Genetics, University of Illinois at Chicago, Chicago, IL, USA
[5]The Jesse Brown VA Medical Center, Chicago, IL, USA
[6]Department of Nuclear Medicine, Yonsei University College of Medicine, Seoul, South Korea
[7]Department of Surgery, University of California Los Angeles, Los Angeles, CA, USA
[8]California NanoSystems Institute, University of California Los Angeles, Los Angeles, CA, USA
[9]David Geffen School of Medicine, University of California Los Angeles, Los Angeles, CA, USA
[10]Jonsson Comprehensive Cancer Center, University of California Los Angeles, Los Angeles, CA, USA
[11]These authors contributed equally
[12]Lead Contact
*Correspondence: cradu@mednet.ucla.edu
https://doi.org/10.1016/j.chembiol.2019.10.012

SUMMARY

Biosynthesis of the pyrimidine nucleotide uridine monophosphate (UMP) is essential for cell proliferation and is achieved by the activity of convergent *de novo* and salvage metabolic pathways. Here we report the development and application of a cell-based metabolic modifier screening platform that leverages the redundancy in pyrimidine metabolism for the discovery of selective UMP biosynthesis modulators. In evaluating a library of protein kinase inhibitors, we identified multiple compounds that possess nucleotide metabolism modifying activity. The JNK inhibitor JNK-IN-8 was found to potently inhibit nucleoside transport and engage ENT1. The PDK1 inhibitor OSU-03012 (also known as AR-12) and the RAF inhibitor TAK-632 were shown to inhibit the therapeutically relevant *de novo* pathway enzyme DHODH and their affinities were unambiguously confirmed through *in vitro* assays and co-crystallization with human DHODH.

INTRODUCTION

The redundant and plastic nature of metabolic networks is a significant obstacle in the targeting of cancer metabolism. This redundancy manifests in two ways; the first is the expression of multiple enzymes that perform identical biochemical reactions, such as the hexokinase isozymes which each phosphorylate glucose (Xu et al., 2018); the second is the existence of convergent metabolic pathways that produce a common metabolite from unique precursors. Such convergent metabolic nodes have been noted in nucleotide (Le et al., 2017), lipid (cholesterol) (York et al., 2015), and amino acid (aspartate) metabolism (Garcia-Bermudez et al., 2018).

Despite these difficulties, the development of metabolism modifiers remains a robust area of research. One such therapeutically relevant target is pyrimidine nucleotide biosynthesis, which consists of nucleoside salvage (NSP) and *de novo* (DNP) pathways that converge to generate uridine monophosphate (UMP), the common precursor for all pyrimidine nucleotides (Okesli et al., 2017). The NSP allows for the scavenging of uridine (rU) from the extracellular environment, shuttling it into the cell via nucleoside transporters where it is phosphorylated by uridine-cytidine kinases (UCKs) to produce UMP. UCK2 is thought to be the primary NSP kinase, given its 20-fold higher catalytic efficiency compared with UCK1 (Van Rompay et al., 2001). The DNP is a six-step process that utilizes glutamine, aspartate, bicarbonate, and glucose to produce UMP through the action of three enzymes: trifunctional CAD, electron transport chain-linked dihydroorotate dehydrogenase (DHODH), and bifunctional UMP synthase (UMPS). Among DNP enzymes, DHODH in particular has emerged as a therapeutic target in multiple cancers including pancreatic ductal adenocarcinoma (PDAC) (Madak et al., 2019; Sykes et al., 2016; Santana-Codina et al., 2018). In addition, over 90 patent applications involving DHODH inhibition have been filed in the last decade (Lolli et al., 2018).

In this study, we show that the pyrimidine NSP and DNP are interchangeable in their ability to sustain cancer cell proliferation and that a synthetic lethal phenotype can be achieved through their simultaneous inhibition. We leverage this observation to construct a metabolic modifier screen that allows for the identification of selective modulators of NSP and DNP pathways. In

screening a library of protein kinase inhibitors, we identified multiple compounds with nucleotide metabolism-modifying activity. We show that the c-Jun N-terminal kinase (JNK) inhibitor JNK-IN-8 is a potent inhibitor of rU transport that is vital for NSP function, and that the 3-phosphoinositide-dependent protein kinase 1 (PDK1) inhibitor OSU-03012 (also known as AR-12) and the pan-RAF inhibitor TAK-632 both bind and inhibit the pyrimidine DNP enzyme DHODH.

RESULTS

Design of a Differential Metabolic Modifier Screen for Identification of Modulators of Pyrimidine Nucleotide Metabolism

While the UMP-DNP and -NSP are interchangeable in their ability to sustain cell proliferation, their relative activity at baseline (when both pathways are functional) is poorly defined. *De novo* pyrimidine biosynthesis is allosterically inactivated by its end product, UTP, which is also produced by the rU salvage pathway (Evans and Guy, 2004). This allosteric control functions at the level of the CPSase activity of the trifunctional protein CAD, which performs the first committed step in *de novo* pyrimidine biosynthesis (Figure S1A). To quantitatively evaluate the discrete activities of the pyrimidine *de novo* and salvage pathways, we modified and applied a liquid chromatography-tandem mass spectrometry (LC-MS/MS) assay previously used by our group to track the contribution of stable isotope-labeled glucose and deoxycytidine to newly replicated DNA (Le et al., 2017). In this assay, cells are cultured in the presence of [$^{13}C_6$]glucose (to track DNP activity) and 10 μM [$^{13}C_9$;$^{15}N_2$]rU (to track NSP activity). Their DNA is then extracted and hydrolyzed and the abundance of stable isotope-labeled nucleosides is evaluated using LC-MS/MS in the multiple reaction monitoring mode (Figure S1B). We applied this assay to a panel of cancer cell lines and observed a heterogeneous degree of total labeling ([$^{13}C_6$]glucose + [$^{13}C_9$;$^{15}N_2$]rU) in the deoxycytidine compartment of DNA (DNA-C) after 24 h (Figure S1C). Consistent with the aforementioned model in which UTP produced by rU savage allosterically impairs *de novo* biosynthesis, we found that the fractional contribution of [$^{13}C_9$;$^{15}N_2$]rU exceeded that of [$^{13}C_6$]glucose in all models tested (Figure S1D). Interestingly, we found heterogeneity in the relative contribution of [$^{13}C_6$]glucose and [$^{13}C_9$;$^{15}N_2$]rU to DNA-C across the cell line panel, which likely reflects differential expression or regulation of the various transporters, kinases, nucleotidases, and phosphorylases involved in rU salvage. Importantly, we confirmed that the contribution of [$^{13}C_6$]glucose to DNA-C could be blocked by NITD-982, an established DHODH inhibitor (Bonavia et al., 2011), and likewise the contribution of [$^{13}C_9$;$^{15}N_2$]rU could be prevented by the FDA-approved nucleoside transport inhibitor dipyridamole (DPA) (Figure S1E) (Young et al., 2013). Collectively, these results suggest that, under the conditions tested, both the UMP-DNP and -NSP pathways are simultaneously, but not equally, active.

Although redundant routes for UMP biosynthesis can complicate targeting, impaired proliferation resulting from simultaneous restriction of both *de novo* and salvage pathways can be leveraged for the identification of selective DNP or NSP activity modifiers (Figure S1F). A metabolic modifier screen was developed for the discovery of small-molecule modulators of UMP production by leveraging this biosynthetic redundancy. This cell-based platform concurrently tests the effects of small-molecule compounds on the proliferation of cells cultured in baseline (both NSP and DNP active), NSP-only, and DNP-only conditions (Figure 1A). Compounds which inhibit proliferation in baseline conditions are classified as non-specific inhibitors, those which selectively inhibit proliferation in NSP-only conditions are NSP inhibitors, while those that selectively inhibit growth in DNP-only conditions are DNP inhibitors. The screen design was validated using NITD-982 (which inhibits the DNP) and DPA (which inhibits the NSP), with Cell TiterGlo (CTG) utilized to evaluate proliferation impairment (Figure S1G) (Wang et al., 2011).

Cancer cell lines exhibited varying degrees of sensitivity to DHODH inhibition (as determined by doubling time normalized proliferation inhibition) and were all rescued by rU supplementation (Figure S2) (Hafner et al., 2016). MIAPACA2 PDAC cells were utilized for the screen due to their ability to maintain baseline proliferation levels in NSP-only or DNP-only conditions, while also exhibiting a significant decrease in proliferation upon simultaneous NSP and DNP inhibition (Figure S3A). A library of 430 protein kinase inhibitors was chosen for evaluation, the rationale being 2-fold. First, it was hypothesized that our synthetic lethality screen may identify compounds that indirectly target pyrimidine metabolism through regulatory signal transduction pathway inhibition. Second, because a substantial fraction of kinase inhibitors are ATP-mimetics and, therefore, resemble nucleotides, we predicted that protein kinase inhibitors may possess secondary, non-canonical targets within nucleotide metabolism. Consistently, several protein kinase inhibitors, specifically those exhibiting similarities with imatinib's phenylamino pyrimidine scaffold, and a subset of p38 MAPK inhibitors, exhibit activity against nucleoside transporters (Damaraju et al., 2016; Huang et al., 2002). This kinase inhibitor library was screened at seven-point dose response in duplicates. Composite NSP and DNP pathway selectivity scores were calculated for each compound as the sum of condition-specific anti-proliferative effects across the dose range (Data S1; Figure S3B). Phenotypic screen quality was monitored using the Z-factor metric (Zhang et al., 1999) (Figure S3C).

The JNK inhibitor JNK-IN-8, the BTK inhibitor CNX-774, and the VEGFR inhibitor AMG-706 were active in the NSP-only condition, exhibiting positive NSP selectivity scores (Figure 1B). The selectivity of these hits for the NSP was unique among inhibitors of JNK (Figures 1C and 1D), BTK, and VEGFR (Figures S3D–S3F), indicating this phenotype likely did not result from on-target effects. The PDK1 inhibitor OSU-03012 (also known as AR-12) and the pan-RAF inhibitor TAK-632 elicited potent and selective inhibition of proliferation in the DNP-only condition (Figure 1E) (Zhu et al., 2004; Okaniwa et al., 2013). Among the 4 PDK1 inhibitors and 14 RAF inhibitors tested, OSU-03012 and TAK-632 were unique in their ability to selectively inhibit the DNP, suggesting that this effect is not the consequence of on-target activity (Figures 1F–1H).

Microplate immunofluorescence microscopy nuclei scoring analysis of MIAPACA2 cells stained with Hoechst 33342 was performed as an orthogonal evaluation of hit compound activity. These studies confirmed the culture condition selectivity of our hits and validated the results of the CTG-based screen (Figures S3G and S3H). In addition, we performed CTG analysis and

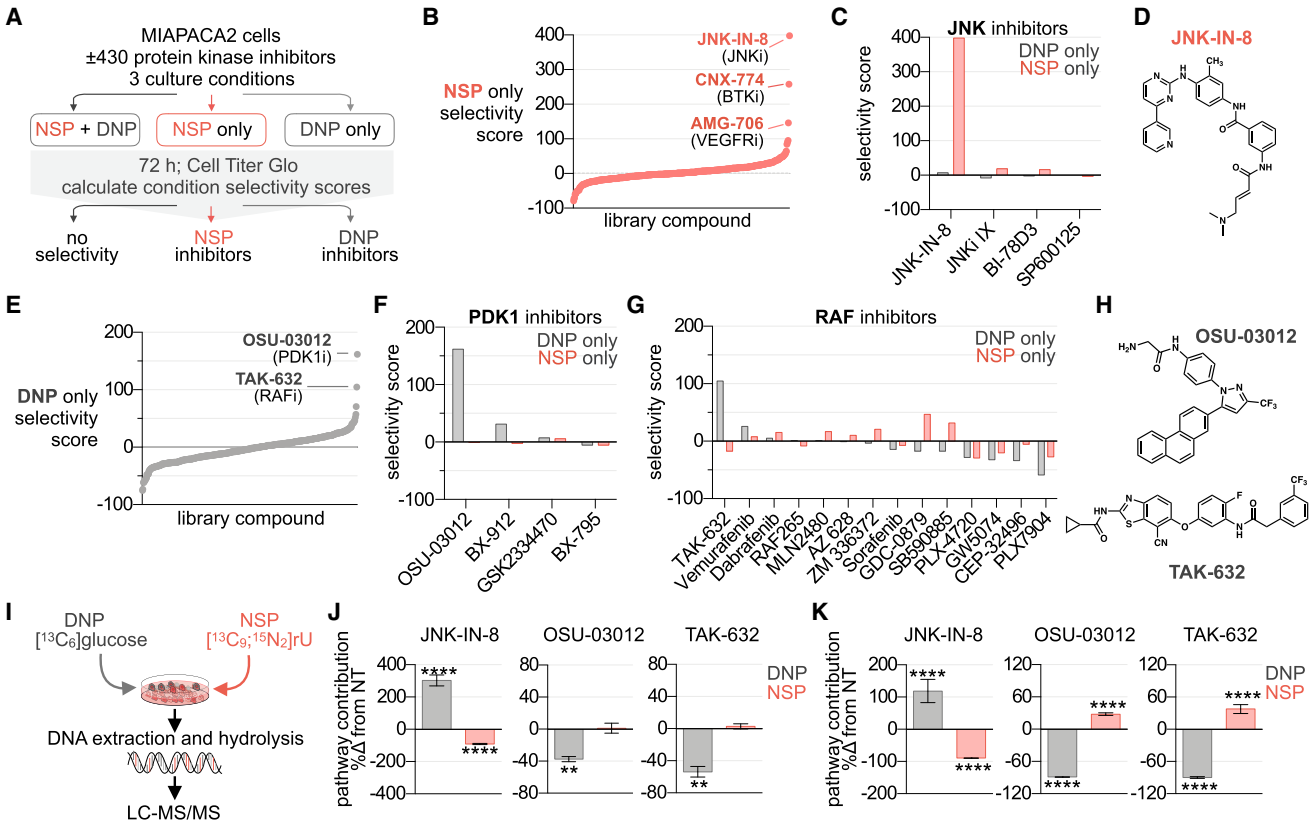

Figure 1. Identification of Nucleotide Metabolism Modulators in a Small Molecule Protein Kinase Inhibitor Library

(A) Phenotypic screening strategy. The impact of 430 protein kinase inhibitors on cell proliferation was evaluated in MIAPACA2 cells cultured in 3 distinct conditions; (i) NSP + DNP (medium + 10 μM rU); (ii) NSP only (medium +10 μM rU + 1 μM NITD-982); or (iii) DNP only (medium alone). Proliferation vinhibition was evaluated using Cell Titer Glo (CTG) following 72 h treatment (library compounds were tested at 7-point dose response; n = 2).

(B) Waterfall plot ranking library compounds by NSP pathway selectivity score.

(C) Summary of NSP and DNP selectivity scores across library compounds annotated as JNK inhibitors.

(D) Structure of JNK-IN-8.

(E) Waterfall plot ranking library compounds by DNP pathway selectivity score.

(F and G) Summary of NSP and DNP selectivity scores across library compounds annotated as PDK1 (F) or RAF (G) inhibitors .

(H) Structures of OSU-03012 and TAK-632.

(I) Experimental design to track contribution of UMP-DNP and -NSP pathways to newly replicated DNA using stable isotope-labeled metabolite tracers.

(J and K) LC-MS/MS analysis of [$^{13}C_6$]glucose (5.5 mM) and [$^{13}C_9$;$^{15}N_2$] rU (10 μM) utilization for DNA-C replication in MIAPACA2 (J) or JURKAT (K) cells treated + 1 μM JNK-IN-8 + 5 μM OSU-03012 or + 5 μM TAK-632 for 24 h (NT, not-treated; mean ± SD; n = 3; unpaired t test; **p < 0.01, ****p < 0.0001).

trypan blue exclusion cell scoring in a second cancer cell line, JURKAT, to confirm hit selectivity (Figures S3I and S3J).

In addition to its non-redundant role in *de novo* pyrimidine nucleotide biosynthesis, DHODH functions as an electron donor in the mitochondrial electron transport chain (Fang et al., 2013). To exclude the possibility that the selective activity of JNK-IN-8 reflects an interaction with NITD-982 at the level of electron transport chain modulation, we synthesized and evaluated N-phosphonacetyl-L-aspartate (PALA), an inhibitor of CAD, which functions upstream of DHODH (Collins and Stark, 1971; Peters, 2018). We determined that JNK-IN-8 inhibits JURKAT cell proliferation when both PALA and rU are present in the culture media, supporting that its selective activity results from the inhibition of uridine salvage (Figure S4A).

We next applied our LC-MS/MS stable isotope tracking approach to evaluate the impact of JNK-IN-8, OSU-03012, and TAK-632 on the incorporation of [$^{13}C_6$]glucose and [$^{13}C_9$;$^{15}N_2$] rU into newly replicated DNA (Figure 1I). In MIAPACA2 cells, we found that JNK-IN-8 blocked the NSP contribution while triggering a compensatory upregulation of the DNP. Conversely, OSU-03012 and TAK-632 selectively impaired DNP contribution (Figure 1J). Similar selectivity was observed in JURKAT cells, where both OSU-03012 and TAK-632 blocked DNP contribution while inducing compensatory upregulation of the NSP (Figure 1K).

JNK-IN-8 Inhibits Nucleoside Uptake

Although three protein kinase inhibitors were identified as selective inhibitors of the pyrimidine NSP, JNK-IN-8 was exceptionally potent, with NSP-condition IC_{50} values in the low nanomolar range. We reasoned that the activity of JNK-IN-8 could arise from either the inhibition of nucleoside shuttling across the plasma membrane, which is achieved by nucleoside transporters, or through the inhibition of nucleoside phosphorylation

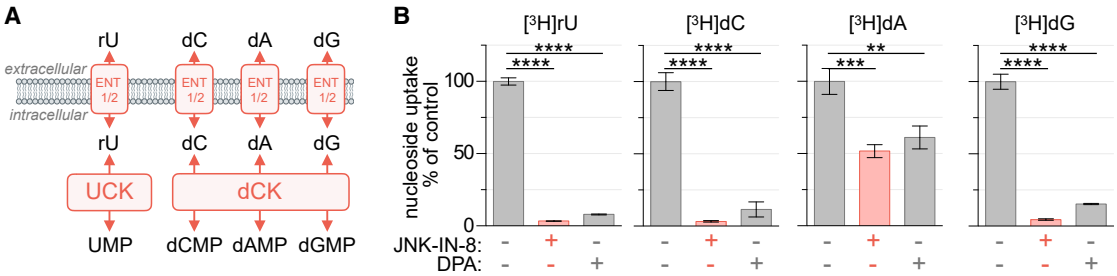

Figure 2. JNK-IN-8 Inhibits Nucleoside Uptake

(A) Uridine salvage pathway activity can be prevented by inhibition of either nucleoside transporters or kinases.

(B) Uptake of [^{3}H]rU, [^{3}H]dC, [^{3}H]dA (+ 10 μM dCF), and [^{3}H]dG (+ 1 μM BCX-1777) in MIAPACA2 cells following 2 h incubation ± 1 μM JNK-IN-8 or 1 μM dipyridamole (DPA) (18.5 kBq; mean ± SD; n = 3; one-way ANOVA corrected for multiple comparisons by Bonferroni adjustment; **p < 0.01, ***p < 0.001, ****p < 0.0001).

by nucleoside kinases. To determine the level at which JNK-IN-8 is active, we determined the effects of JNK-IN-8 on the uptake of a panel of [^{3}H]-labeled purine (dA, dG) and pyrimidine nucleosides (rU, dC) in MIAPACA2 cells. These nucleosides rely upon the same nucleoside transporters to enter the cell but require unique kinases for conversion into their respective monophosphate forms and intracellular accumulation. UCKs are required for the phosphorylation of rU while deoxycytidine kinase (dCK) is required for the phosphorylation of both purine and pyrimidine deoxyribonucleosides including dC, dA, and dG (Figure 2A) (Le et al., 2017). We found that JNK-IN-8 prevented the uptake of all nucleosides tested, but exhibited greater potency toward rU and dC. Importantly, JNK-IN-8 exhibits a selectivity pattern similar to the established ENT1 inhibitor DPA (Figure 2B). We confirmed JNK-IN-8 inhibited the uptake of both rU and dC with similar potency (33 and 31 nM, respectively), further suggesting that the compound inhibits nucleoside transport (Figure S4C). In addition, JNK-IN-8 treatment prevented the antiproliferative effects of gemcitabine (dFdC), a dCK-dependent nucleoside analog prodrug which relies upon nucleoside transporters for its activation, in a dose-dependent manner (Figure S4D) (Mackey et al., 1998). A similar pattern of dA, dG, rU, and dC uptake inhibition by JNK-IN-8 and DPA was observed in a second cell line, the murine pancreatic cancer model KP4662 (Figures S4E and S4F) (Byrne et al., 2016).

Seven nucleoside transporters have been described and categorized into two families. Concentrative nucleoside transporters (CNT1-3; SLC28A1-3) are unidirectional inward transporters that co-transport Na^+. Equilibrative nucleoside transporters (ENT1-4; SLC29A1-4) are bidirectional, energy-independent, and accept a broad range of purine and pyrimidine nucleosides (Young et al., 2013). We evaluated the expression of these transporters in MIAPACA2 and JURKAT cells and found that ENT1 (SLC29A1) is the predominantly expressed transporter in both models (Figure S4G) (Fernandez-Banet et al., 2016). ENT1 is an established transporter of a variety of nucleosides including natural purine and pyrimidine nucleosides as well as therapeutic analogs such as dFdC (Young et al., 2013). We next utilized the cellular thermal shift assay (CETSA), an approach that leverages the altered thermostability of proteins following ligand binding, to confirm ENT1 engagement by JNK-IN-8 (Figure S4H) (Martinez Molina and Nordlund, 2016). Collectively, these results suggest that JNK-IN-8 inhibits UMP-NSP activity by interfering with the transport of rU.

OSU-03012 and TAK-632 Target *De Novo* UMP Biosynthesis and Activate the DNA Replication Stress Response Pathway

Two protein kinase inhibitors, TAK-632 and OSU-03012, were identified as potent and selective inhibitors of MIAPACA2 proliferation in the DNP-only culture condition (Figure 1E). We reasoned that these compounds could restrict pyrimidine biosynthesis by targeting CAD, DHODH, or UMPS–the three enzymes essential for *de novo* UMP biosynthesis (Figure 3A). In MIAPACA2 cells cultured in the DNP-only condition both OSU-03012 and TAK-632 induced S-phase arrest, a phenotype associated with dNTP biosynthesis levels insufficient to sustain DNA replication and is the result of activation of intra-S-phase cell-cycle signaling checkpoints (Figure 3B). This effect was rescued by orotate (the product of DHODH) supplementation and completely reversed by rU supplementation (Figures 3B and 3C). These data implicated DHODH as a likely target of both OSU-03012 and TAK-632. DHODH catalyzes one of three committed steps within the DNP and is an established druggable protein (Madak et al., 2019). In addition, both OSU-03012 and TAK-632 possess fluorine substituents, which have been shown to stabilize bioactive conformations of DHODH inhibitors (Bonomo et al., 2013; Baumgartner et al., 2006). In an *in vitro* colorimetric recombinant human DHODH activity assay, TAK-632 and OSU-03012 both inhibited DHODH activity in a dose-dependent manner (Figure 3D) (Baumgartner et al., 2006). Importantly, the response to TAK-632 or OSU-03012 correlated with the response to a known DHODH inhibitor in a panel of 25 pancreatic cancer cell lines (Figure 3E).

OSU-03012 was recently reported to synergize with replication stress response kinase inhibitors in RSK-subtype mutant KRAS cancer models (Yuan et al., 2018). However, after confirming that OSU-03012 binds DHODH, we hypothesized that the observed synergy resulted from DHODH inhibition rather than PDK1 inhibition. Immunoblot analysis of S6K and S6 phosphorylation, PDK1 downstream targets, confirmed that GSK-2334470, a known PDK1 inhibitor, potently blocked PDK1 while OSU-03012 triggered S345 CHEK1 phosphorylation, a replication stress biomarker, only in the absence of rU (Figure 3F).

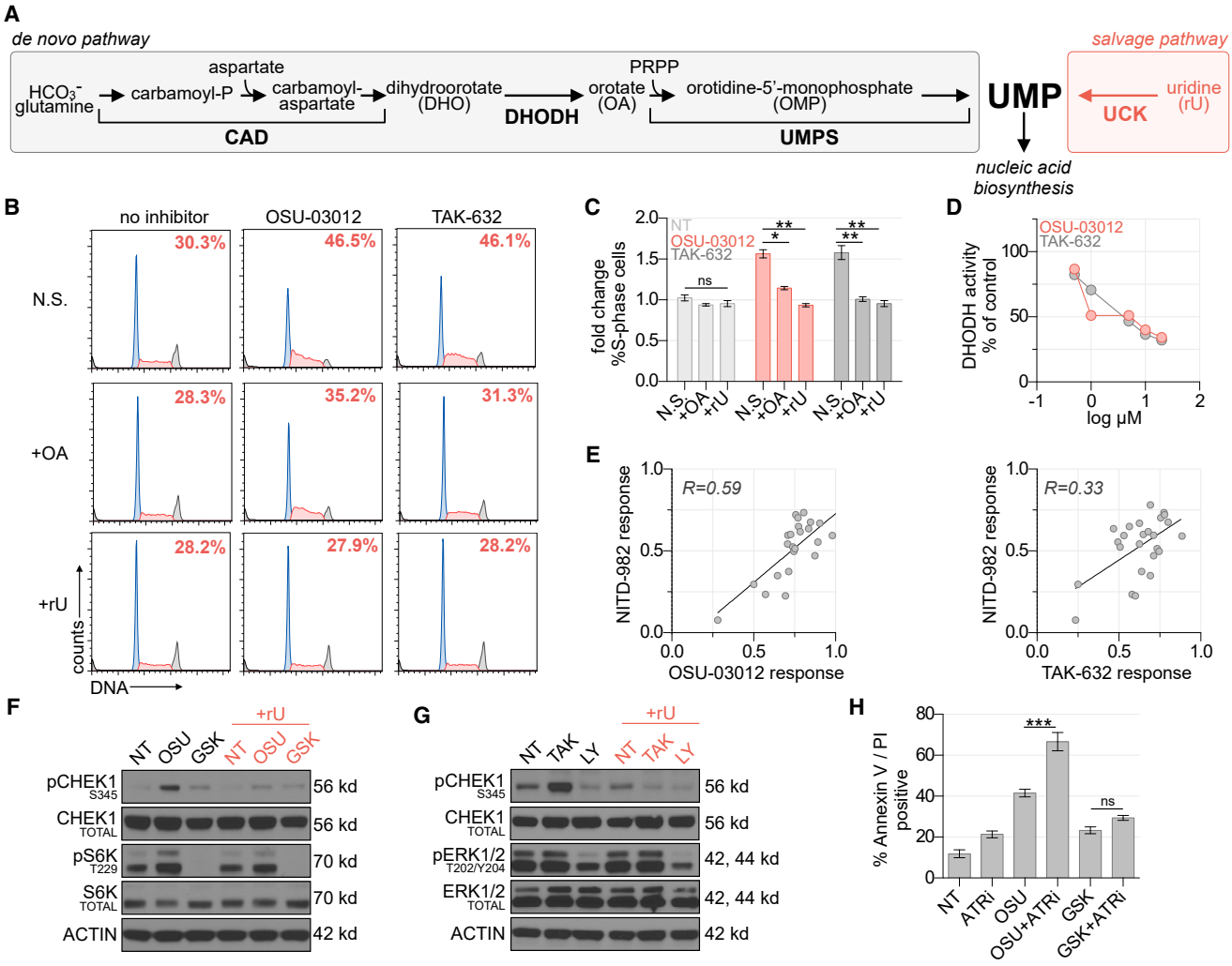

Figure 3. OSU-03012 and TAK-632 Inhibit DHODH and Activate the DNA Replication Stress Response Pathway

(A) Schematic of UMP biosynthesis via *de novo* and salvage pathways.

(B) Propidium iodide cell-cycle analysis of MIAPACA2 PDAC cells treated ± 5 μM TAK-632 or ± 5 μM OSU-03012 and supplemented with 50 μM orotate (OA) or 10 μM rU (N.S., no supplement). Insert indicates percent of S-phase cells.

(C) Summary of fold changes in S-phase cells from (B) (mean ± SD; n = 2; one-way ANOVA corrected for multiple comparisons by Bonferroni adjustment, ns, not significant; *p < 0.05, **p < 0.01).

(D) *In vitro* DHODH enzyme assay performed in the presence of OSU-03012 or TAK-632.

(E) Correlation between DHODH inhibitor (1 μM NITD-982) and OSU-03012 (3.17 μM) or TAK-632 (3.17 μM) response across a panel of 25 PDAC cell lines determined using CTG following 72 h treatment. Response calculated as doubling time normalized proliferation inhibition. Pearson correlation coefficient is indicated.

(F) Immunoblot analysis of MIAPACA2 cells treated ± 1 μM PDK1 inhibitor GSK-2334470 (GSK) ±1 μM OSU-03012 (OSU) ± 10 μM rU for 24 h.

(G) Immunoblot analysis of MIAPACA2 cells treated ± 10 μM RAF inhibitor LY3009120 (LY) ± 10 μM TAK-632 (TAK) ± 10 μM rU for 24 h.

(H) Annexin V/PI flow cytometry analysis of MIAPACA2 PDAC cells treated ± 1 μM OSU-03012 (OSU) or 1 μM GSK-2334470 (GSK) ± 500 nM VE-822 (ATRi) ± 25 μM rU for 72 h (mean ± SD; n = 2; one-way ANOVA corrected for multiple comparisons by Bonferroni adjustment; ns, not significant; **p < 0.01, ***p < 0.001).

Similarly, TAK-632 only triggered CHEK1 phosphorylation in the absence of rU, whereas an established pan-RAF inhibitor, LY3009120, which does not trigger paradoxical RAF activation, downregulated ERK1/2 phosphorylation but had no impact on CHEK1 phosphorylation (Figure 3G) (Peng et al., 2015). Consistently, we found that neither GSK-2334470 nor LY3009120 induced S-phase arrest at doses where we observed downregulation of their target substrates, whereas a known DHODH inhibitor induced potent S-phase accumulation that was completely reversed by rU supplementation (Figures S4I and S4J). To complement our evaluation of replication stress response biomarker induction we performed an assessment of DNA damage induced by OSU-03012, TAK-632, and the ATR inhibitor VE-822 as a positive control using γ-H2A.X flow cytometry. We found that while OSU-03012 and TAK-632 trigger activation of the replication stress response, they do not significantly induce γ-H2A.X. We hypothesize that activation of the replication stress response pathway by OSU-03012 or TAK-632 limits DNA double-strand

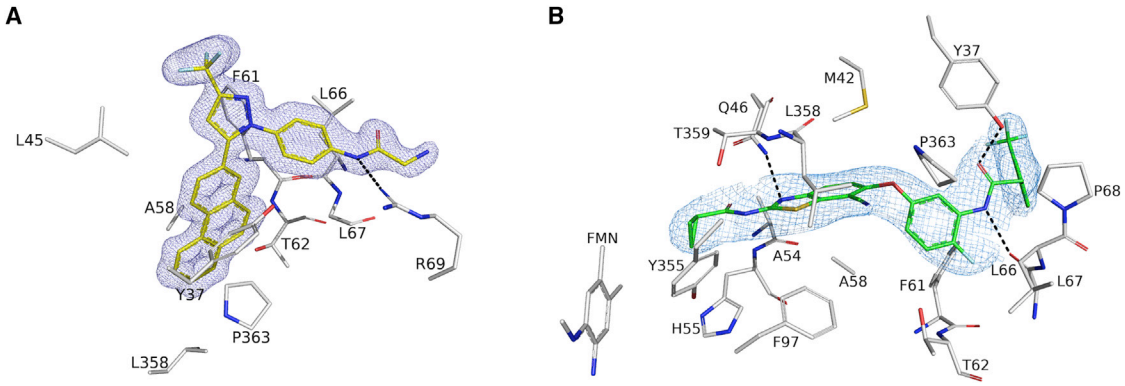

Figure 4. OSU-03012 and TAK-632 bind DHODH

Crystal Structure of DHODH with compounds OSU-03012 (A) or TAK-632 (B). 2mFo-DFc electron density for OSU-03012 (carbons in yellow) or TAK-632 (carbons in green) contoured at 1σ. Dashed black lines represent hydrogen bonds between DHODH and its ligands. Interacting residues as predicted by LigPlot+ are shown and labeled.

breaks by preventing the collapse of stalled replication forks (Figure S4K) (Zeman and Cimprich, 2014).

To investigate the interactions between DHODH, PDK1 and replication stress response inhibitors, we treated MIAPACA2 cells with VE-822 (Le et al., 2017), an inhibitor of the replication stress response kinase ataxia telangiectasia and Rad3-related (ATR), and either OSU-03012 or GSK-2334470 for 72 h. A synergistic increase in apoptotic cells was observed when OSU-03012 and an ATR inhibitor were combined, whereas the combination of GSK-2334470 and VE-822 demonstrated only a nominal increase as determined by annexin V/propidium iodide (PI) flow cytometry (Figure 3H). Taken together, these data suggest that replication stress triggered by OSU-03012 is the consequence of DHODH inhibition rather than inhibition of its canonical target.

Co-crystal Structures of OSU-03012 and TAK-632 in Complex with Human DHODH

To determine the molecular interactions between DHODH and its putative inhibitors, complete co-crystallization datasets were obtained and processed to 1.4 and 2.7 Å for OSU-03012 and TAK-632, respectively (Table S1). Both compounds bind in a hydrophobic channel composed by two N-domain α helices through which ubiquinone travels, a mechanism consistent with previously identified DHODH inhibitors (Baumgartner et al., 2006). A long-range hydrogen bond between Arg 69 and OSU-03012 helps orient the molecule to the hydrophobic pocket where the phenanthrene moiety inserts, while the remainder of the molecule lies on the outer surface of DHODH, blocking the hydrophobic channel (Figure 4A) (PDB: 6OC0). Three hydrogen bonds stabilize TAK-632 in the same hydrophobic pocket: two with Tyr 37 and Leu 66 help stabilize the inhibitor at the opening of the channel, while a third with Gln 46 helps pull the inhibitor deep into the pocket (Figure 4B) (PDB: 6OC1).

DISCUSSION

Our screening strategy expands upon previously described "nutrient-sensitized" genetic and small-molecule cell-based screening approaches which leveraged the production of a proliferation-enabling metabolite by parallel and redundant metabolic networks to identify selective metabolism modifiers (Arroyo et al., 2016; Gohil et al., 2010). UMP biosynthesis (i.e., pyrimidine metabolism) proved to be compatible with this screening framework as UMP is produced by convergent (*de novo* and salvage) pathways, and UMP depletion triggers a quantifiable change in cellular proliferation.

JNK-IN-8, developed as an irreversible inhibitor of c-Jun N-terminal kinases 1, 2, and 3 with low-nanomolar affinity, was the most potent of three uridine salvage inhibitors identified (Zhang et al., 2012). Our data demonstrate that JNK-IN-8 also functions as a potent inhibitor of uridine and deoxycytidine transport and engages the nucleoside transporter ENT1 (SLC29A1). We conclude that JNK-IN-8 should not be used in conjunction with compounds which rely upon nucleoside transport, such as the anticancer agent gemcitabine, in research or therapy settings.

In addition to their role in pyrimidine salvage, equilibrative nucleoside transporters are well studied for their ability to regulate levels of the immuno-modulatory metabolite adenosine. ENT1 inhibitors increase extracellular adenosine levels that signal through the P1 purinergic receptor and are used clinically for the treatment of hypertension, among other disorders (Young et al., 2013). Thus, the development of potent and selective inhibitors of ENT1 is an active area of investigation.

The recently reported co-crystal structure of ENT1 in complex with two small-molecule inhibitors (NBMPR and dilazep) provided new insight into the molecular mechanism of nucleoside transport and suggested that structurally diverse ENT1 inhibitors possess unique modes of inhibition (Wright and Lee, 2019). ENT1 contains ten cysteine residues and ENT1-mediated uridine transport can be inhibited by covalent modification of Cys416 by *N*-ethylmaleimide (Yao et al., 2018). Intriguingly, the two highest-scoring NSP inhibitors in our screen, JNK-IN-8 and the BTK inhibitor CNX-774, each contain a reactive acrylamide group and are cysteine-targeting drugs. Future work will explore the mechanism of ENT1 inhibition by JNK-IN-8 with a specific focus on the contribution of covalent interactions.

Positron emission tomography (PET) imaging is a powerful approach to monitor cellular metabolism *in vivo*, and several nucleoside analog PET probes have been developed including both pyrimidine ([^{18}F]FAC and [^{18}F]FLT) and purine analogs ([^{18}F]CFA) (Radu et al., 2008; Shields et al., 1998; Kim et al., 2016). Interestingly, ENT1 knockout mice exhibit significantly higher plasma thymidine but also paradoxically higher levels of thymidine analog [^{18}F]FLT uptake in the spleen and bone marrow compared with wild-type controls (Paproski et al., 2010). Discrepancies between *in vitro* and *in vivo* findings could result from shifts in nucleoside gradients or differential expression of nucleoside transporters mediated by factors absent from traditional cell culture systems Future work will focus on exploring the utility of nucleoside analog PET as a pharmacodynamic biomarker for ENT inhibitor activity *in vivo*.

The structurally and functionally unrelated OSU-03012 and TAK-632 were identified as inhibitors of the pyrimidine DNP. A recent report described the ability of OSU-03012 and analogs to inhibit virus propagation via pyrimidine nucleotide biosynthesis inhibition, specifically implicating modulation of DHODH activity (Yang et al., 2018). Our work substantiates these findings and confirms engagement of DHODH by OSU-03012 and TAK-632 through crystallography studies. Notably, our studies show that OSU-03012 and TAK-632 bind in the same hydrophobic tunnel of DHODH as known inhibitors brequinar and teriflunomide (the active metabolite of leflunomide). This suggests that these two protein kinase inhibitors compete with ubiquinone, a redox partner of DHODH, which traverses this hydrophobic tunnel to regenerate FMN from $FMNH_2$. By competitively inhibiting the binding of ubiquinone, these compounds prevent DHODH from completing its redox cycle and effectively abrogate its activity.

OSU-03012 has orphan drug designation in the European Union for treatment of tularemia and cryptococcosis. We hypothesize that its effectiveness in these indications stems from its ability to inhibit DHODH, rather than from "on-target" effects against PDK1. Indeed, DHODH inhibitors have demonstrated efficacy against viruses, such as dengue virus and respiratory syncytial virus (Bonavia et al., 2011; Yang et al., 2018; Wang et al., 2011). In anticancer settings, OSU-03012 was recently demonstrated to synergize with CHEK1 inhibitors in KRAS-mutant cancers which was initially attributed to its ability to inhibit PDK1 (Yuan et al., 2018). However, our data show that GSK-2334470, a PDK1 inhibitor more potent than OSU-03012, displayed little synergy with ATR inhibition. In light of our crystallographic data, we conclude that the synergy observed between OSU-03012 and ATR inhibition is likely a result of the DHODH-inhibitory ability of the former. Taken together, our data suggest that DHODH inhibitors may have utility in oncology, particularly if used in conjunction with ATR inhibitors or other DNA damage response/replication stress response pathway inhibitors (Le et al., 2017).

In summary, we designed and applied a metabolic modifier screen which identified multiple protein kinase inhibitors with secondary, non-canonical targets within pyrimidine metabolism. Similarly constructed phenotypic screens designed against other metabolic networks containing convergent nodes may find use in drug discovery campaigns or in repurposing screens using existing compounds.

SIGNIFICANCE

The pyrimidine nucleotide uridine monophosphate (UMP) is essential for cell proliferation and is produced by convergent *de novo* and salvage biosynthetic pathways that utilize unique metabolic precursors. This redundancy can be leveraged for the identification of selective metabolic pathway inhibitors using cell-based phenotypic metabolic modifier screens. In screening a library of 430 protein kinase inhibitors, multiple compounds that possess selective UMP metabolism-modifying activity were identified. This activity was subsequently shown to be unrelated to inhibition of the canonical targets of these inhibitors and is the consequence of their binding to and inhibition of nucleotide metabolism proteins, namely DHODH or ENT1. We describe a modular screening strategy that can be utilized for drug discovery and adapted for the identification of small-molecule inhibitors of additional convergent metabolic pathways.

STAR★METHODS

Detailed methods are provided in the online version of this paper and include the following:

- KEY RESOURCES TABLE
- LEAD CONTACT AND MATERIALS AVAILABILITY
  - Lead Contact
  - Materials Availability Statement
- EXPERIMENTAL MODEL AND SUBJECT DETAILS
  - Cell Culture
  - Drugs
- METHOD DETAILS
  - Protein Kinase Inhibitor Phenotypic Screen
  - Cell Titer Glo Viability Analysis
  - Trypan Blue Exclusion Cell Viability Analysis
  - Immunofluorescence Microscopy Cell Scoring
  - Mass Spectrometry Analysis
  - [^{3}H]-labeled Metabolite Uptake Assays
  - Flow Cytometry
  - Gene Cloning, Protein Expression, and Purification of DHODH in E.coli Cells
  - Recombinant DHODH Enzyme Assay
  - Crystallization of DHODH with OSU-03012 and TAK-632
  - Phasing/Structural Solution, Refinement Strategies and Model Validation
  - Immunoblot Analysis
  - CETSA Analysis
- QUANTIFICATION AND STATISTICAL ANALYSES
- DATA AND CODE AVAILABILITY

SUPPLEMENTAL INFORMATION

Supplemental Information can be found online at https://doi.org/10.1016/j.chembiol.2019.10.012.

ACKNOWLEDGMENTS

We thank Bobby Tofig and Constance Yuen at the UCLA Molecular Shared Screening Resource for assistance performing the high-throughput screen.

We thank Dr. Steven Mittelman for his critical review of this manuscript. We thank all members of the Ahmanson Translational Imaging Division at UCLA for their advice, technical expertise, and support. This work was supported by the National Science Foundation Graduate Research Fellowship Program (grant no. DGE-1650504 to E.W.R.).

AUTHOR CONTRIBUTIONS

E.R.A. and C.G.R. designed the study and analyzed data. E.R.A. and R.D. designed and performed the high-throughput chemical genomics screen. M.A.D. prepared recombinant DHODH protein. V.L. performed recombinant DHODH activity studies. S.P. performed flow cytometry studies. E.W.R. synthesized NITD-982 and PALA. M.A.D. and A.L. performed protein crystallography. T.M.L. performed mass spectrometry studies. L.W., R.S., J.S., W.K., J.R.C., and A.C. provided technical assistance and gave advice on experimental design. M.E.J., J.C., and T.R.D. provided reagents and gave advice on study design. E.R.A., E.W.R., and C.G.R. wrote the manuscript. C.G.R. supervised the study.

DECLARATION OF INTERESTS

C.G.R. and J.C. are co-founders of Sofie Biosciences and Trethera Corporation. M.E.J. is a co-founder of Trethera Corporation. They and the University of California (UC) hold equity in Sofie Biosciences and Trethera Corporation. The intellectual property developed by C.G.R., J.C., and M.E.J. and licensed by UC to Sofie Biosciences and Trethera Corporation was not used in this study.

Received: May 1, 2019
Revised: August 30, 2019
Accepted: October 25, 2019
Published: November 13, 2019

REFERENCES

Arroyo, J.D., Jourdain, A.A., Calvo, S.E., Ballarano, C.A., Doench, J.G., Root, D.E., and Mootha, V.K. (2016). A genome-wide CRISPR death screen identifies genes essential for oxidative phosphorylation. Cell Metab. *24*, 875–885.

Baumgartner, R., Walloschek, M., Kralik, M., Gotschlich, A., Tasler, S., Mies, J., and Leban, J. (2006). Dual binding mode of a novel series of DHODH inhibitors. J. Med. Chem. *49*, 1239–1247.

Bonavia, A., Franti, M., Pusateri Keaney, E., Kuhen, K., Seepersaud, M., Radetich, B., Shao, J., Honda, A., Dewhurst, J., Balabanis, K., et al. (2011). Identification of broad-spectrum antiviral compounds and assessment of the druggability of their target for efficacy against respiratory syncytial virus (RSV). Proc. Natl. Acad. Sci. U S A *108*, 6739–6744.

Bonomo, S., Tosco, P., Giorgis, M., Lolli, M., and Fruttero, R. (2013). The role of fluorine in stabilizing the bioactive conformation of dihydroorotate dehydrogenase inhibitors. J. Mol. Model. *19*, 1099–1107.

Byrne, K.T., Leisenring, N.H., Bajor, D.L., and Vonderheide, R.H. (2016). CSF-1R-dependent lethal hepatotoxicity when agonistic CD40 antibody is given before but not after chemotherapy. J. Immunol. *197*, 179–187.

Campbell, D.O., Yaghoubi, S.S., Su, Y., Lee, J.T., Auerbach, M.S., Herschman, H., Satyamurthy, N., Czernin, J., Lavie, A., and Radu, C.G. (2012). Structure-guided engineering of human thymidine kinase 2 as a positron emission tomography reporter gene for enhanced phosphorylation of non-natural thymidine analog reporter probe. J. Biol. Chem. *287*, 446–454.

Collins, K.D.S., and Stark, G.R. (1971). Aspartate transcarbamylase. Interaction with the transition state analogue N-(phosphonacetyl)-L-aspartate. J. Biol. Chem. *246*, 6599–6605.

Damaraju, V.L., Weber, D., Kuzma, M., Cass, C.E., and Sawyer, M.B. (2016). Selective inhibition of human equilibrative and concentrative nucleoside transporters by BCR-ABL kinase inhibitors: identification of key hENT1 amino acid residues for interaction with BCR-ABL kinase inhibitors. J. Biol. Chem. *291*, 18809–18817.

Das, P., Deng, X., Zhang, L., Roth, M.G., Fontoura, B.M., Phillips, M.A., and De Brabander, J.K. (2013). SAR based optimization of a 4-quinoline carboxylic acid analog with potent anti-viral activity. ACS Med. Chem. Lett. *4*, 517–521.

Davies, M., Heikkilä, T., McConkey, G.A., Fishwick, C.W., Parsons, M.R., and Johnson, A.P. (2009). Structure-based design, synthesis, and characterization of inhibitors of human and *Plasmodium falciparum* dihydroorotate dehydrogenases. J. Med. Chem. *52*, 2683–2693.

Deng, X., Kokkonda, S., El Mazouni, F., White, J., Burrows, J.N., Kaminsky, W., Charman, S.A., Matthews, D., Rathod, P.K., and Phillips, M.A. (2014). Fluorine modulates species selectivity in the triazolopyrimidine class of *Plasmodium falciparum* dihydroorotate dehydrogenase inhibitors. J. Med. Chem. *57*, 5381–5394.

Erra, M., Moreno, I., Sanahuja, J., Andrés, M., Reinoso, R.F., Lozoya, E., Pizcueta, P., Godessart, N., and Castro-Palomino, J.C. (2011). Biaryl analogues of teriflunomide as potent DHODH inhibitors. Bioorg. Med. Chem. Lett. *21*, 7268–7272.

Evans, D.R., and Guy, H.I. (2004). Mammalian pyrimidine biosynthesis: fresh insights into an ancient pathway. J. Biol. Chem. *279*, 33035–33038.

Fang, J., Uchiumi, T., Yagi, M., Matsumoto, S., Amamoto, R., Takazaki, S., Yamaza, H., Nonaka, K., and Kang, D. (2013). Dihydro-orotate dehydrogenase is physically associated with the respiratory complex and its loss leads to mitochondrial dysfunction. Biosci. Rep. *33*, e00021.

Fernandez-Banet, J., Esposito, A., Coffin, S., Horvath, I.B., Estrella, H., Schefzick, S., Deng, S., Wang, K., AChing, K., Ding, Y., et al. (2016). OASIS: web-based platform for exploring cancer multi-omics data. Nat. Methods *13*, 9–10.

Garcia-Bermudez, J., Baudrier, L., La, K., Zhu, X.G., Fidelin, J., Sviderskiy, V.O., Papagiannakopoulos, T., Molina, H., Snuderl, M., Lewis, C.A., et al. (2018). Aspartate is a limiting metabolite for cancer cell proliferation under hypoxia and in tumours. Nat. Cell Biol. *20*, 775–781.

Gohil, V.M., Sheth, S.A., Nilsson, R., Wojtovich, A.P., Lee, J.H., Perocchi, F., Chen, W., Clish, C.B., Ayata, C., Brookes, P.S., and Mootha, V.K. (2010). Nutrient-sensitized screening for drugs that shift energy metabolism from mitochondrial respiration to glycolysis. Nat. Biotechnol. *28*, 249–255.

Hafner, M., Niepel, M., Chung, M., and Sorger, P.K. (2016). Growth rate inhibition metrics correct for confounders in measuring sensitivity to cancer drugs. Nat. Methods *13*, 521–527.

Huang, M., Wang, Y., Collins, M., Gu, J.J., Mitchell, B.S., and Graves, L.M. (2002). Inhibition of nucleoside transport by p38 MAPK inhibitors. J. Biol. Chem. *277*, 28364–28367.

Hurt, D.E., Sutton, A.E., and Clardy, J. (2006). Brequinar derivatives and species-specific drug design for dihydroorotate dehydrogenase. Bioorg. Med. Chem. Lett. *16*, 1610–1615.

Kim, W., Le, T.M., Wei, L., Poddar, S., Bazzy, J., Wang, X., Uong, N.T., Abt, E.R., Capri, J.R., Austin, W.R., et al. (2016). [^{18}F]CFA as a clinically translatable probe for PET imaging of deoxycytidine kinase activity. Proc. Natl. Acad. Sci. U S A *113*, 4027–4032.

Ladds, M.J.G.W., van Leeuwen, I.M.M., Drummond, C.J., Chu, S., Healy, A.R., Popova, G., Pastor Fernández, A., Mollick, T., Darekar, S., Sedimbi, S.K., et al. (2018). Publisher correction: a DHODH inhibitor increases p53 synthesis and enhances tumor cell killing by p53 degradation blockage. Nat. Commun. *9*, 2071.

Laskowski, R.A., and Swindells, M.B. (2011). LigPlot+: multiple ligand-protein interaction diagrams for drug discovery. J. Chem. Inf. Model. *51*, 2778–2786.

Le, T.M., Poddar, S., Capri, J.R., Abt, E.R., Kim, W., Wei, L., Uong, N.T., Cheng, C.M., Braas, D., Nikanjam, M., et al. (2017). ATR inhibition facilitates targeting of leukemia dependence on convergent nucleotide biosynthetic pathways. Nat. Commun. *8*, 241.

Lewis, T.A., Sykes, D.B., Law, J.M., Muñoz, B., Rustiguel, J.K., Nonato, M.C., Scadden, D.T., and Schreiber, S.L. (2016). Development of ML390: a human DHODH inhibitor that induces differentiation in acute myeloid leukemia. ACS Med. Chem. Lett. *7*, 1112–1117.

Liu, S., Neidhardt, E.A., Grossman, T.H., Ocain, T., and Clardy, J. (2000). Structures of human dihydroorotate dehydrogenase in complex with antiproliferative agents. Structure *8*, 25–33.

Lolli, M.L., Sainas, S., Pippione, A.C., Giorgis, M., Boschi, D., and Dosio, F. (2018). Use of human dihydroorotate dehydrogenase (hDHODH) inhibitors in autoimmune diseases and new perspectives in cancer therapy. Recent Pat. Anticancer Drug Discov. *13*, 86–105.

Mackey, J.R., Mani, R.S., Selner, M., Mowles, D., Young, J.D., Belt, J.A., Crawford, C.R., and Cass, C.E. (1998). Functional nucleoside transporters are required for gemcitabine influx and manifestation of toxicity in cancer cell lines. Cancer Res. *58*, 4349–4357.

Madak, J.T., Bankhead, A., 3rd, Cuthbertson, C.R., Showalter, H.D., and Neamati, N. (2019). Revisiting the role of dihydroorotate dehydrogenase as a therapeutic target for cancer. Pharmacol. Ther. *195*, 111–131.

Martinez Molina, D., and Nordlund, P. (2016). The cellular thermal shift assay: a novel biophysical assay for in situ drug target engagement and mechanistic biomarker studies. Annu. Rev. Pharmacol. Toxicol. *56*, 141–161.

McLean, L.R., Zhang, Y., Degnen, W., Peppard, J., Cabel, D., Zou, C., Tsay, J.T., Subramaniam, A., Vaz, R.J., and Li, Y. (2010). Discovery of novel inhibitors for DHODH via virtual screening and X-ray crystallographic structures. Bioorg. Med. Chem. Lett. *20*, 1981–1984.

Morris, A.D., and Cordi, A.A. (1997). A new, efficient, two step procedure for the preparation of the antineoplastic agent sparfosic acid. Synth. Commun. *27*, 1259–1266.

Nathanson, D.A., Armijo, A.L., Tom, M., Li, Z., Dimitrova, E., Austin, W.R., Nomme, J., Campbell, D.O., Ta, L., Le, T.M., et al. (2014). Co-targeting of convergent nucleotide biosynthetic pathways for leukemia eradication. J. Exp. Med. *211*, 473–486.

Okaniwa, M., Hirose, M., Arita, T., Yabuki, M., Nakamura, A., Takagi, T., Kawamoto, T., Uchiyama, N., Sumita, A., Tsutsumi, S., et al. (2013). Discovery of a selective kinase inhibitor (TAK-632) targeting pan-RAF inhibition: design, synthesis, and biological evaluation of C-7-substituted 1,3-benzothiazole derivatives. J. Med. Chem. *56*, 6478–6494.

Okesli, A., Khosla, C., and Bassik, M.C. (2017). Human pyrimidine nucleotide biosynthesis as a target for antiviral chemotherapy. Curr. Opin. Biotechnol. *48*, 127–134.

Paproski, R.J., Wuest, M., Jans, H.S., Graham, K., Gati, W.P., McQuarrie, S., McEwan, A., Mercer, J., Young, J.D., and Cass, C.E. (2010). Biodistribution and uptake of 3′-deoxy-3′-fluorothymidine in ENT1-knockout mice and in an ENT1-knockdown tumor model. J. Nucl. Med. *51*, 1447–1455.

Peng, S.B., Henry, J.R., Kaufman, M.D., Lu, W.P., Smith, B.D., Vogeti, S., Rutkoski, T.J., Wise, S., Chun, L., Zhang, Y., et al. (2015). Inhibition of RAF isoforms and active dimers by LY3009120 leads to anti-tumor activities in RAS or BRAF mutant cancers. Cancer Cell *28*, 384–398.

Peters, G.J. (2018). Antipyrimidine effects of five different pyrimidine de novo synthesis inhibitors in three head and neck cancer cell lines. Nucleosides Nucleotides Nucleic Acids *37*, 329–339.

Radu, C.G., Shu, C.J., Nair-Gill, E., Shelly, S.M., Barrio, J.R., Satyamurthy, N., Phelps, M.E., and Witte, O.N. (2008). Molecular imaging of lymphoid organs and immune activation by positron emission tomography with a new [^{18}F]-labeled 2′-deoxycytidine analog. Nat. Med. *14*, 783–788.

Sainas, S., Pippione, A.C., Lupino, E., Giorgis, M., Circosta, P., Gaidano, V., Goyal, P., Bonanni, D., Rolando, B., Cignetti, A., et al. (2018). Targeting myeloid differentiation using potent 2-hydroxypyrazolo[1,5-a]pyridine scaffold-based human dihydroorotate dehydrogenase inhibitors. J. Med. Chem. *61*, 6034–6055.

Santana-Codina, N., Roeth, A.A., Zhang, Y., Yang, A., Mashadova, O., Asara, J.M., Wang, X., Bronson, R.T., Lyssiotis, C.A., Ying, H., and Kimmelman, A.C. (2018). Oncogenic KRAS supports pancreatic cancer through regulation of nucleotide synthesis. Nat. Commun. *9*, 4945.

Shields, A.F., Grierson, J.R., Dohmen, B.M., Machulla, H.J., Stayanoff, J.C., Lawhorn-Crews, J.M., Obradovich, J.E., Muzik, O., and Mangner, T.J. (1998). Imaging proliferation in vivo with [F-18]FLT and positron emission tomography. Nat. Med. *4*, 1334–1336.

Sykes, D.B., Kfoury, Y.S., Mercier, F.E., Wawer, M.J., Law, J.M., Haynes, M.K., Lewis, T.A., Schajnovitz, A., Jain, E., Lee, D., et al. (2016). Inhibition of dihydroorotate dehydrogenase overcomes differentiation blockade in acute myeloid leukemia. Cell *167*, 171–186.e15.

Van Rompay, A.R., Norda, A., Lindén, K., Johansson, M., and Karlsson, A. (2001). Phosphorylation of uridine and cytidine nucleoside analogs by two human uridine-cytidine kinases. Mol. Pharmacol. *59*, 1181–1186.

Wallace, A.C., Laskowski, R.A., and Thornton, J.M. (1995). LIGPLOT: a program to generate schematic diagrams of protein-ligand interactions. Protein Eng. *8*, 127–134.

Walse, B., Dufe, V.T., Svensson, B., Fritzson, I., Dahlberg, L., Khairoullina, A., Wellmar, U., and Al-Karadaghi, S. (2008). The structures of human dihydroorotate dehydrogenase with and without inhibitor reveal conformational flexibility in the inhibitor and substrate binding sites. Biochemistry *47*, 8929–8936.

Wang, Q.Y., Bushell, S., Qing, M., Xu, H.Y., Bonavia, A., Nunes, S., Zhou, J., Poh, M.K., Florez de Sessions, P., Niyomrattanakit, P., et al. (2011). Inhibition of dengue virus through suppression of host pyrimidine biosynthesis. J. Virol. *85*, 6548–6556.

Wright, N.J., and Lee, S.Y. (2019). Structures of human ENT1 in complex with adenosine reuptake inhibitors. Nat. Struct. Mol. Biol. *26*, 599–606.

Xu, S., Catapang, A., Doh, H.M., Bayley, N.A., Lee, J.T., Braas, D., Graeber, T.G., and Herschman, H.R. (2018). Hexokinase 2 is targetable for HK1 negative, HK2 positive tumors from a wide variety of tissues of origin. J. Nucl. Med. https://doi.org/10.2967/jnumed.118.212365.

Yang, C.F., Gopula, B., Liang, J.J., Li, J.K., Chen, S.Y., Lee, Y.L., Chen, C.S., and Lin, Y.L. (2018). Novel AR-12 derivatives, P12-23 and P12-34, inhibit flavivirus replication by blocking host de novo pyrimidine biosynthesis. Emerg. Microbes Infect. *7*, 187.

Yao, S.Y.M., Ng, A.M.L., Cass, C.E., and Young, J.D. (2018). Role of cysteine 416 in *N*-ethylmaleimide sensitivity of human equilibrative nucleoside transporter 1 (hENT1). Biochem. J. *475*, 3293–3309.

York, A.G., Williams, K.J., Argus, J.P., Zhou, Q.D., Brar, G., Vergnes, L., Gray, E.E., Zhen, A., Wu, N.C., Yamada, D.H., et al. (2015). Limiting cholesterol biosynthetic flux spontaneously engages type I IFN signaling. Cell *163*, 1716–1729.

Young, J.D., Yao, S.Y., Baldwin, J.M., Cass, C.E., and Baldwin, S.A. (2013). The human concentrative and equilibrative nucleoside transporter families, SLC28 and SLC29. Mol. Aspects Med. *34*, 529–547.

Yuan, T.L., Amzallag, A., Bagni, R., Yi, M., Afghani, S., Burgan, W., Fer, N., Strathern, L.A., Powell, K., Smith, B., et al. (2018). Differential effector engagement by oncogenic KRAS. Cell Rep. *22*, 1889–1902.

Zeman, M.K., and Cimprich, K.A. (2014). Causes and consequences of replication stress. Nat. Cell Biol. *16*, 2–9.

Zhang, J.H., Chung, T.D.Y., and Oldenburg, K.R. (1999). A simple statistical parameter for use in evaluation and validation of high throughput screening assays. J. Biomol. Screen. *4*, 67–73.

Zhang, T., Inesta-Vaquera, F., Niepel, M., Zhang, J., Ficarro, S.B., Machleidt, T., Xie, T., Marto, J.A., Kim, N., Sim, T., et al. (2012). Discovery of potent and selective covalent inhibitors of JNK. Chem. Biol. *19*, 140–154.

Zhu, J., Huang, J.W., Tseng, P.H., Yang, Y.T., Fowble, J., Shiau, C.W., Shaw, Y.J., Kulp, S.K., and Chen, C.S. (2004). From the cyclooxygenase-2 inhibitor celecoxib to a novel class of 3-phosphoinositide-dependent protein kinase-1 inhibitors. Cancer Res. *64*, 4309–4318.

STAR★METHODS

KEY RESOURCES TABLE

REAGENT or RESOURCE	SOURCE	IDENTIFIER
Chemicals, Peptides, and Recombinant Proteins		
DMEM	Corning	10-107-CV
RPMI	Corning	10-040-CV
Glucose-Free DMEM	Corning	17-207-CV
Glucose-Free RPMI	Corning	10-043-CV
Dialyzed Fetal Bovine Serum	Gibco	26-400-044
Kinase Inhibitor Library	SelleckChem	L1200
JNK-IN-8	SelleckChem	S4901
TAK-632	Cayman Chemicals	16285
OSU-03012	SelleckChem	S1106
GSK2334470	Cayman Chemicals	18095
AMG-706	Cayman Chemicals	17671
CNX-774	Cayman Chemicals	21475
NITD-982	This Study	N/A
PALA	This study	N/A
Dipyridamole	Sigma-Aldrich	D9766
Gemcitabine	SelleckChem	S1714
dCF	Sigma-Aldrich	SML0508
BCX-1777	MedChemExpress	HY-16209
Uridine	Sigma-Aldrich	U3003
[^{3}H]dC	Moravek	MT673
[^{3}H]rU	PerkinElmer	NET367250UC
[^{3}H]dG	Moravek	MT507
[^{3}H]dA	Moravek	MT641
[$^{13}C_6$]glucose	Cambridge Isotope Laboratories	CLM-1396-1
[$^{13}C_9$;$^{15}N_2$]rU	Cambridge Isotope Laboratories	CNLM-3809-PK
Orotate	Sigma-Aldrich	O2750
VE-822	SelleckChem	S7102
Hoechst 33342	ThermoFisher Scientific	62249
RIPA Protein Lysis Buffer	Boston BioProducts	BP-115
Laemmli Loading Dye	Boston BioProducts	BP-110R
4-12% Bis-Tris Gels	ThermoFisher Scientific	NP0336
Nitrocellulose Membrane	ThermoFisher Scientific	88018
Nonfat Dry Milk	ThermoFisher Scientific	M-0841
Tris-Buffered Saline	ThermoFisher Scientific	50-751-7046
Tween-20	Sigma-Aldrich	P9416
SuperSignal West Pico	ThermoFisher Scientific	34580
SuperSignal West Femto	ThermoFisher Scientific	34095
Autoradiography Film	Denville	E3012
Halt Protease Inhibitor Cocktail	ThermoFisher Scientific	PI78430
Halt Phosphatase Inhibitor Cocktail	ThermoFisher Scientific	PI78428
Cytofix/Cytoperm Buffer	BD Biosciences	554722
Perm/Wash Buffer	BD Biosciences	554723
White Opaque 384-well Plates	VWR	781080

(*Continued on next page*)

Continued

REAGENT or RESOURCE	SOURCE	IDENTIFIER
Black Clear Bottom 384-well Plates	VWR	781086
Zymo-Spin IC Columns	Zymo Research	C1004
DNA Degradase Plus	Zymo Research	E2021
Antibodies		
ACTIN	Cell Signaling Technology	3700
PHOSPHO CHEK1 S345	Cell Signaling Technology	2348
TOTAL CHEK1	Cell Signaling Technology	2360
PHOSPHO S6K T229	Novus Biologicals	MAB2964-SP
TOTAL S6K	Cell Signaling Technology	9202
PHOSPHO ERK1/2 T202/Y204	Cell Signaling Technology	9101
TOTAL ERK1/2	Cell Signaling Technology	9102
PHOSPHO H2A.X S139 - FITC	MilliporeSigma	16-202A
VINCULIN	Cell Signaling Technology	13901
ENT1	Novus Biologicals	NBP1-50508
ANTI-RABBIT IgG, HRP-LINKED	Cell Signaling Technology	7074
ANTI-MOUSE IgG, HRP-LINKED	Cell Signaling Technology	7076
Recombinant DHODH protein	This study	N/A
Dihydroorotate	Sigma-Aldrich	D1728
Coenzyme Q_{10}	Sigma-Aldrich	C9538
4-TFMBAO	Sigma-Aldrich	422231
$K_3[Fe(CN)_6]$	Sigma-Aldrich	244023
K_2CO_3	Sigma-Aldrich	P5833
Experimental Models: Cell Lines		
JURKAT	ATCC	TIB-152
MIAPACA2	ATCC	CRL-1420
CCRF-CEM	ATCC	CCL-119
KP4662	Gift from Dr. Vonderheide (UPenn)	N/A
Software and Algorithms		
Graphpad Prism	Graphpad Software	https://www.graphpad.com/scientific-software/prism/
FlowJo 7.6	TreeStar	https://www.flowjo.com
MetaXpress	Molecular Devices	https://www.moleculardevices.com
Critical Commercial Assay		
BCA Assay	ThermoFisher Scientific	23225
AnnexinV-FITC Apoptosis Detection Kit	BD Biosciences	556547
Cell Titer Glo	Promega	G7572
MycoPlasma Detection Kit	Sigma-Aldrich	MP0025
Deposited Data		
OSU-03012:DHODH protein structure	This study	6OC0
TAK-632:DHODH protein structure	This study	6OC1
Other		
ImageXpress Confocal Micro	Molecular Devices	N/A
ViCell Cell Viability Analyzer	Beckman Coulter	N/A
6460 Triple Quadruple Mass Spectrometer	Agilent	N/A

LEAD CONTACT AND MATERIALS AVAILABILITY

Lead Contact

Reagent or resource requests should be submitted to the lead contact, Caius G. Radu (cradu@mednet.ucla.edu).

Materials Availability Statement

All unique/stable reagents generated in this study are available from the Lead Contact with a completed Materials Transfer Agreement.

EXPERIMENTAL MODEL AND SUBJECT DETAILS

Cell Culture

Human cancer cells including MIAPACA2 (male) and JURKAT (male) were evaluated between passages 3 and 20 and maintained in antibiotic-free DMEM or RPMI +10% FBS at 37°C in 5% CO_2. Mycoplasma contamination was monitored using the PCR-based Venor Mycoplasma kit. PDAC cell lines were acquired either from a commercial vendor (ATCC, DSMZ) or from collaborators (KP4662 from Dr. Vonderheide, UPenn, sex not available). Cell line identity was independently authenticated by PCR.

Drugs

Drug stocks were prepared in DMSO or H_2O and diluted fresh in cell culture media for treatments. NITD-982 was synthesized as previously described (Bonavia et al., 2011). N-phosphonacetyl-L-aspartate (PALA) was synthesized as previously described (Morris and Cordi, 1997).

METHOD DETAILS

Protein Kinase Inhibitor Phenotypic Screen

A library of 430 protein kinase inhibitors was arrayed in polypropylene 384-well plates at 200x concentrations covering a 7-point concentration range (corresponding to 1x concentrations: 5μM, 1.65μM, 550nM, 185nM, 61.5nM, 20.6nM, 6.85nM). 25μl per well of condition-specific growth media (DNP+NSP: media +10 μM rU; DNP: media alone; NSP: media +10 μM rU + 1 μM NITD-982) was plated in opaque-white 384-well plates using a BioTek multidrop liquid handler. Protein kinase inhibitors were added by 250 nL pin-tool transfer (BioMek FX, Beckman-Coulter) and inhibitor/media mixtures were incubated at room temperature for 30 m. 25 μL of a 40,000 cells/mL MIAPACA2 suspension (for 1000 cells / well) was subsequently added to each well. After 72 h, 50 μL of Cell Titer Glo reagent diluted 1:4 in dH_2O was added to each well and luminescence was measured using a Wallac plate reader (Perkin Elmer). Each condition was assayed in duplicate (n = 2) and % proliferation values were calculated by normalizing experimental wells to plate negative controls and averaging replicate values. Composite pathway selectivity synergy scores for each test compound were defined as the sum of the excess over additivity (% proliferation inhibition observed - % proliferation inhibition expected) between individual protein kinase inhibitor concentrations across the 7-point concentration range. Z factor scores for individual assay plates were calculated using eight positive and eight negative control wells on each plate as previously described (Zhang et al., 1999). All plates gave a Z factor > 0.5 (Figure S3C).

Cell Titer Glo Viability Analysis

Cells were plated at $1x10^3$ cells / well in 50 μl in white opaque 384-well plates and treated as described. Following seeding or incubation for 72 h, 50 μl of Cell Titer Glo reagent (diluted 1:5 in dH_2O) was added to each well, plates were incubated at room temperature for 5 m and luminescence was measured using a microplate luminescence reader. Proliferation rate normalized growth inhibition was calculated using the previously described GR metric (Hafner et al., 2016). Experimental CTG reading (CTG_x) were normalized to vehicle treated control readings at seeding (CTG_{t0}) or following 72 h of culture (CTG_{ctrl}).

$$GR(x) = 2^{\log_2(CTG_x/CTG_{t0})/\log_2(CTG_{ctrl}/CTG_{t0})} - 1$$

Trypan Blue Exclusion Cell Viability Analysis

JURKAT cells were plated $1x10^5$ cells/well in 6-well plates in 2 mL of media and treated with 10 μM rU, 1 μM NITD-982, 100 nM JNK-IN-8, 1 μM OSU-03012 or 1 μM TAK-632. Following incubation for 72 h, 500 uL of cell cultures were collected for trypan blue exclusion cell viability analysis using a ViCell analyzer. All conditions were tested in biological triplicate. Trypan blue-negative population counts are reported.

Immunofluorescence Microscopy Cell Scoring

MIAPACA2 cells were plated at 1000 cells/well in black-walled clear-bottom 384 well plates in 50 μL of media and treated as indicated with n = 4 replicate wells per condition. After 72 h of drug exposure 50 μL of 10 μg/mL Hoechst 33342 dye diluted in culture media was added to microplate wells. Following a 30 m incubation at 37C images were acquired using a ImageXpress Micro Confocal High-Content Imaging System at 10x magnification and 1 image/well. Analysis was performed using the *Cell Scoring Application Module* in the MetaXpress analysis software. Nuclei counts for treatment groups were normalized to control wells.

Mass Spectrometry Analysis

For analysis of stable isotope-labeled metabolite incorporation into newly replicated DNA, cells were cultured in glucose-free DMEM (for MIAPACA2 cells) or RPMI (for JURKAT cells) media supplemented with 10% dialyzed FBS, 4 mM glutamine, 1 g/L [$^{13}C_6$]glucose, 10 μM [$^{13}C_9$; $^{15}N_2$]rU and treated as indicated.

Genomic DNA was extracted using the Quick-gDNA MiniPrep kit and hydrolyzed to nucleosides using the DNA Degradase Plus kit, following manufacturer-supplied instructions. In the final step of DNA extraction, 50 μL of water was used to elute the DNA into 1.5 mL microcentrifuge tubes. A nuclease solution (5 μL; 10X buffer/DNA Degradase PlusTM/water, 2.5/1/1.5, v/v/v) was added to 20 μL of the eluted genomic DNA in an HPLC injector vial. The samples were incubated overnight at 37°C.

Hydrolyzed DNA was diluted 1/1 with solvent A (water/acetonitrile/formic acid, 95/5/0.1, v/v) and analyzed using a modified version of a previously reported method (Le et al., 2017; Nathanson et al., 2014) in which aliquots of the solution (15 μL) were injected onto a porous graphitic carbon column (Thermo Hypercarb, 100 x 2.1 mm, 5 micron particle size) equilibrated in solvent A and eluted (300 μL/min) with an increasing concentration of solvent B (acetonitrile/water/formic acid, 90/10/0.1). The HPLC timetable, in terms of min/%B, is the following: 0/0, 5/0, 12/20, 15/30, 17/50, 19/50, 20/0, 24/0. The effluent from the column was directed to Agilent Jet Stream connected Agilent 6460 QQQ operating in the positive ion MRM mode. After verification of retention times using authentic standards, the peak areas of the protonated nucleoside/protonated base fragment ion transitions for each of the nucleosides were recorded with instrument manufacturer-supplied software.

[^{3}H]-labeled Metabolite Uptake Assays

Radioactive probe uptake assays were conducted as previously described (Campbell et al., 2012). Briefly, cells were pretreated with JNK-IN-8 or DPA for 2 h before incubation with 18.5 kBq of [^{3}H]-labeled probe for 2 h. For purine uptake assays, cells were cultured in the presence of 10 μM dCF (for [^{3}H]-dA) or 1 μM BCX-1777 (for [^{3}H]-dG) to prevent nucleoside catabolism. Following incubation, cells were washed with PBS and lysed. Cell lysate radioactivity was measured using a beta-counter (Perkin-Elmer).

Flow Cytometry

All flow cytometry data were acquired on five-laser BD LSRII, and analyzed using FlowJo software.

AnnexinV/PI

Treated PDAC cells were washed with PBS and incubated with AnnexinV and propidium iodide diluted in 1x Annexin binding buffer. 20,000 events were collected per sample.

Propidium Iodide Cell Cycle

Treated PDAC cells were washed with PBS and suspended in propidium iodide cell cycle staining solution (100 μg/ml propidium iodide; 20 μg/ml Ribonuclease A). 10,000 events were collected per sample.

pH2A.X$_{S139}$

Treated cells were collected by trypsinization, incubated with Cytofix/Cytoperm reagent for 15 m at 4C, washed with PBS and incubated in 100 μL PermWash buffer for 15 m at 4C. Cells were washed with 1 mL Perm/Wash buffer, resuspended in 50 μL of staining solution (1:800 dilution of FITC-conjugated pH2AX$_{S139}$ antibody diluted in Perm/Wash buffer) and incubated for 20 m at 25C protected from light. Stained cells were washed and incubated in 500 μL of DAPI staining solution (1 μg/mL DAPI in PBS) before acquisition.

Gene Cloning, Protein Expression, and Purification of DHODH in E.coli Cells

Primers were ordered to add NdeI (AGAGAACAGATTGGTGGTCATATGATGGCCACGGGAGATGAG) upstream of residue 29 (after the mitochondrial membrane associated loop) and BamHI (TCGGGCTTTGTTAGCAGCCGGATCCTTACCTCCGATGATCTGCTCC) after the stop codon to insert into N-terminal His-Sumo pET 14b vector. This clone, His-Sumo-DHODH 29-395 (subsequently referred to as DHODH) was successfully inserted into the vector in XL1-blue cells for vector propagation.

The vector was transformed into C41(DE3) cells for production. Cells were grown at 37°C in 2xYT medium supplemented with 100 μg/mL ampicillin (Amp), treated with 0.1 mM isopropyl β-D-1-thiogalactopyranoside (IPTG) at an OD600 nm of 0.6-0.8, and then cultured for an additional 18 h at 18°C. Cells were harvested by centrifugation, washed with 200 mM NaCl and 25 mM Tris pH 7.5, and pelleted at 5000 rpm for 20 min before storage at -20°C. 6.7g/L of cell pellet was obtained.

DHODH was purified according to known purification conditions (Baumgartner et al., 2006). The cell pellet was resuspended in lysis buffer (50 mM Tris pH 7.5; 600 mM NaCl; 0.33% w/v Thesit; 10% Glycerol; 1 mM PMSF) and lysed by sonication on ice. Lysed cells were centrifuged at 58,500 RCF for 45 min at 4°C, and the supernatant was filtered through a 0.45 μM filter and loaded onto a 5-mL His-Trap column pre-equilibrated with buffer A (50 mM Tris pH 7.4; 600 mM NaCl; 0.05% w/v Thesit; 10% Glycerol). The column was washed with buffer A for 70 mL, buffer A with 25 mM imidazole for 50 mL, and buffer A with 50 mM imidazole for 50 mL. The protein was eluted with buffer A with 250 mM imidazole. The eluted fraction was diluted 1:1 with Buffer A. Sumo protease was added and the protein was dialyzed overnight at 4°C against 1L of Buffer A. The dialyzed protein was loaded back onto the His-Trap column equilibrated with buffer A. The cut-DHODH was eluted with buffer A with 50 mM imidazole. The purified protein was concentrated to 5 mL and injected onto S-200 gel filtration column (GE Healthcare) equilibrated with: 50 mM HEPES pH 7.7, 400 mM NaCl, 10% Glycerol, 1 mM EDTA, 0.05 % w/v Thesit. Eluted fractions consistent with monomer size were collected, concentrated, flash frozen, and stored at -80°C.

Recombinant DHODH Enzyme Assay

Evaluation of DHODH inhibition was performed as previously described (Baumgartner et al., 2006). The standard assay mixture contained 50 μM decyclo-ubiquinone, 100 μM dihydroorotate, and 60 μM 2,6-dichloroindophenol (DCIP). The amount of DHODH was 337.4 ng/mL. Measurements were conducted in 50 mM TrisHCl, 150 mM KCl, 0.1% Triton X-100, pH 8.0, at 30°C in a final volume of 1 mL. The components were mixed, and the reaction was started by adding dihydroorotate. The reaction was followed spectrophotometrically by measuring the decrease in absorption at 600 nm for 2.5 min at 30 s intervals. The assay was linear in time and enzyme concentration. Inhibitory studies were conducted in a standard assay with additional variable amounts of inhibitor.

Crystallization of DHODH with OSU-03012 and TAK-632

For co-crystallizaion of DHODH and OSU-03012, crystals were obtained using the same conditions reported in previously published DHODH structures (Lewis et al., 2016; Baumgartner et al., 2006; Das et al., 2013; Davies et al., 2009; Erra et al., 2011; Hurt et al., 2006; Ladds et al., 2018; Liu et al., 2000; McLean et al., 2010; Sainas et al., 2018; Walse et al., 2008), namely 1.6 – 2.6 M ammonium sulfate and 5%–30% glycerol in the well in pH 4.5, with 20 mg/mL DHODH with 2 mM dihydroorotate (DHO), 20.8 mM dodecyldimethyl-N-amineoxide (DDAO), and 400 μM inhibitor. Protein was mixed 1:1 with mother liquor and hanging drops were used at room temperature. Crystals appeared after 48 h and reached maximal size within one week. Molecular replacement used 4OQV (Deng et al., 2014) as the starting model. Interestingly, DHODH-TAK-632 crystals grown in similar conditions to those used for the DHODH-OSU-03012 complex did not show TAK-632 density. As a result, novel DHODH crystallization conditions were identified using commercial screens. For co-crystallization of DHODH with TAK-632, crystals were obtained in conditions of 1.4-1.6 M sodium phosphate, pH 8.2. Protein solution (20 mg/mL DHODH with 2 mM DHO, 20.8 mM DDAO, and 400 μM inhibitor) was mixed 1:1 with mother liquor and hanging drops were used at room temperature. Crystals appeared after 48 h and reached maximal size within one week. The lack of density of the TAK-632 structure in the initial crystallography condition is most likely due to the difference in pH between the conditions, pH 4.5 and pH 8.2 for the OSU-03012 and the TAK-632 structure, respectively. There are multiple hydrogen bonds and potentially labile hydrogens on the TAK-632 structure that at low pH could be protonated and charged, potentially preventing their insertion into the hydrophobic tunnel. Ligplot+ (Laskowski and Swindells, 2011; Wallace et al., 1995) was used to determine hydrophilic and hydrophobic interactions between inhibitors and DHODH molecules.

Phasing/Structural Solution, Refinement Strategies and Model Validation

To phase both crystal structures, we used 4OQV as the starting model, including only Chain A without ligands. Phasing was done by molecular replacement using MOLREP included in the CCP4 software suite. Further refinement was done using restrained refinement using refmac, starting at a 4.0 Å cutoff, running 10 cycles. The cutoff was lowered by 0.5 Å each 10 cycles until highest resolution range was reached. The ligands were built in jLigand and added to the model using Coot. Final refinement was done using refmac. Model validation consisted of using Rampage and Procheck for outlier residues and positions, as well as the PDB validation service upon submission.

Immunoblot Analysis

PBS-washed cell pellets were resuspended in cold RIPA buffer supplemented with protease and phosphatase inhibitors. Protein lysates were normalized using BCA assay, diluted using RIPA and 4x laemmli loading dye, resolved on 4%–12% Bis-Tris gels and electro-transferred to nitrocellulose membranes. After blocking with 5% nonfat milk in TBS + 0.1% Tween-20 (TBS-T), membranes were incubated overnight in primary antibodies diluted (per manufacturers instructions) in 5% BSA in TBS-T. Membranes were washed with TBST-T and incubated with HRP-linked secondary antibodies prepared at a 1:2500 dilution in 5% nonfat dry milk / TBS-T. HRP was activated by incubating membranes with a mixture of SuperSignal Pico and SuperSignal Femto ECL reagents (100:1 ratio). Exposure of autoradiography film was used for detection.

CETSA Analysis

MIAPACA2 cells were cultured in 10 cm plates, washed with PBS, and harvested by cell scraping following addition of 4 mL of lysis buffer (100 mM ammonium sulfate, 400 mM NaCl, 10% glycerol, 0.5% DDM and 1x protease inhibitor cocktail). The cell lysate was collected in a 15 mL conical tube, incubated on ice for 20 m, centrifuged at 5,000xg for 20 m at 4C and protein content of the supernatant was measured. 30 μL of protein lysate was aliquoted into 1.5 mL Eppendorf tubes and treated with either DMSO, JNK-IN-8 or dipyridamole for 30 m on ice. Lysates were subsequently heated at the indicated temperatures using an Eppendorf Thermomixer for 6 m, cooled to room temperature for 3 m and transferred to ice. Heated lysates were centrifuged at 12,000xg for 40 m to pellet the insoluble protein fraction. Supernatants were processed for immunoblot analysis.

QUANTIFICATION AND STATISTICAL ANALYSES

Data are presented as mean ± SD with number of biological replicates indicated. Comparisons of two groups were calculated using indicated unpaired two-tailed Student's t-test and P values less than 0.05 were considered significant. Comparisons of more than two groups were calculated using one-way ANOVA followed by Bonferroni's multiple comparison tests, and P values less than 0.05/m, where m is the total number of possible comparisons, were considered significant.

DATA AND CODE AVAILABILITY

The full kinase inhibitor library phenotypic screen results related to Figure 1 are included as Data S1.

The atomic coordinates and structure factors for the OSU-03012:DHODH and TAK-632:DHODH co-crystal structures reported in this study are deposited to the Protein Data Bank under the accession codes PDB 6OC0 and PDB 6OC1, respectively.